Marine Structures 85 (2022) 103236

Contents lists available at ScienceDirect

Marine Structures

journal homepage: www.elsevier.com/locate/marstruc

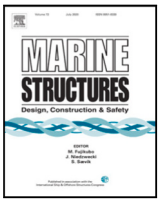

Effect of long periods of corrosion on the fatigue lifetime of offshore mooring chain steel

Paul Qvale [a,*], Håkon O. Nordhagen [b], Sigmund K. Ås [c], Bjørn H. Skallerud [a]

[a] Department of Structural Engineering, Norwegian University of Science and Technology (NTNU), NO-7491 Trondheim, Norway
[b] SINTEF Ocean, P.O. Box 4762 Torgard, NO-7465 Trondheim, Norway
[c] Department of Marine Technology, NTNU, NO-7491 Trondheim, Norway

ARTICLE INFO

Keywords:
Corrosion fatigue
Offshore mooring chain
Seasonal load variations
Fatigue crack growth
Crack tip blunting
Accelerated tests

ABSTRACT

R4-grade mooring chain steel specimens were subjected to alternating phases of saltwater corrosion and air fatigue to replicate seasonal load variations on chains in service. No significant difference in fatigue lifetimes was registered between precorroded specimens subjected to continuous fatigue and those periodically interrupted by phases of accelerated corrosion. Moreover, eight months of natural corrosion of specimens with fatigue cracks did not have a large effect on their remaining fatigue lifetimes. Retardation of fatigue crack growth by crack tip blunting from corrosion is deemed unlikely based on observations from the current work and the literature. Corrosion accelerated by anodic polarization is demonstrated to be unsuitable for replicating natural corrosion of fatigue cracks.

1. Introduction

Position mooring systems are integral parts of floating offshore structures used for oil and gas extraction, wind energy production and aquaculture. Uncoated steel mooring chains experience combined degradation from corrosion and fatigue. Design standards have been established based on laboratory fatigue tests on chain segments, some of which were carried out in seawater [1]. In order to keep test durations at acceptable levels, tests have been conducted at considerably higher loads and frequencies than those experienced by chains in service. While these tests are quite relevant for severe weather conditions, they provide no data for modeling the degradation during calm periods. Since corrosion is a time-dependent process, accelerating the tests means that the effect of corrosion is diminished.

Sea states in the North and Norwegian Sea are characterized by severe winter storms and much calmer summer conditions [2,3]. The calm sea states give rise to stress ranges that are below the cutoff in an accelerated test program. This implies that the intermediate periods between storms are essentially ignored, both in testing and in modeling, although cracks that initiated during a storm may very well be affected by corrosion processes during the calm summer months. This topic is explored in the current paper.

In mooring chains, general and microbiologically influenced corrosion reduce cross sectional areas and introduce macroscopic pits [4,5], increasing stresses globally and locally. Submersion in an electrolyte can accelerate fatigue damage development compared to that in dry air environment: The time of crack initiation is advanced by introduction of surface damage [6] and crack growth rates are believed to be enhanced by hydrogen embrittlement and film-rupture facilitated dissolution at the crack tip [7,8].

Under certain conditions, however, crack growth rates can also be *reduced*, by corrosion product-induced crack closure [7,9]. Moreover, dissolution at the crack tip implies that blunting may occur [7], which could reduce the local stresses at the crack tip.

* Corresponding author.
E-mail address: paul.qvale@ntnu.no (P. Qvale).

https://doi.org/10.1016/j.marstruc.2022.103236
Received 12 November 2021; Received in revised form 25 April 2022; Accepted 30 April 2022
Available online 21 May 2022

Observations of corrosion-induced blunting have been reported from several corrosion fatigue test programs: On the surface of high-strength steel in synthetic seawater at low loads, notch-like pits developed instead of narrow fatigue cracks [10]. For other high-strength steels in distilled water, an attempt to isolate the dissolution mechanism by anodic polarization indicated that blunting was responsible for the observed crack growth retardation [11]. Crack arrest, supposedly from crack tip blunting, has been reported for mild steel with prefabricated fatigue cracks at low load levels and frequency in 3.5% NaCl solution [12]. Also for 2024 aluminum alloy in 3.5% NaCl solution, a retarding effect on crack growth for low load frequency has been shown [13].

It has also been postulated that corrosion-driven dissolution of the free surface that a crack is growing from can retard fatigue damage development by reducing the effective crack depth, or even eliminating the crack altogether [14]. However, it has been demonstrated that crack initiation from a corrosion pit is controlled by the threshold stress intensity factor (SIF) range of an equally sized/deep crack [10,15,16]. Thus, if a short crack in a pit gets eliminated, it would quickly reinitiate from the encompassing, larger and more critical pit.

In the current work, the seasonal load variations on mooring chains have been simplified by assuming that no fatigue-driving load is exerted on the chains during the long "summer" season, and that fatigue is the dominating degradation mechanism during the short "winter" season. During summer, this leaves the corrosion mechanisms to act on fatigue damage over a much larger time scale than during continuous corrosion fatigue. This could lead to more pronounced crack tip blunting, as well as dissolution of a fatigue-damaged chain surface layer, if fatigue is still in the early stages of development. Since build-up of thick oxide layers in a crack in a corrosive environment is facilitated by repeated layer breaking and reforming from contact of the crack surfaces [9], it is assumed here that oxide-induced closure effects during the load-free summer season are limited.

Few records of test programs on alternating fatigue and corrosion exist — none on steel in sea water or other naturally, actively corroding substrate–electrolyte systems. Results from accelerated corrosion phases are difficult to correlate directly to realistic service environments and time scales [17,18], but they can still provide some indications on qualitative effects of corrosion. Alternating tests have been carried out on some aircraft aluminum alloys. Both slightly positive [19] and slightly negative [20] effect of corrosion on fatigue life have been registered. Periodic electropolishing of copper specimens between fatigue phases resulted in up to tenfold improvement in fatigue lifetime compared to continuous-fatigue lifetimes [21]. However, it is unlikely that such extreme trends can be observed for naturally corroding systems that induce corrosion pits.

In this article, two alternating corrosion and fatigue test programs on mooring chain steel are presented. Section 2.1 describes test program 1 (TP1), where the effect of periodic, accelerated corrosion on fatigue lifetimes was explored. The purpose of TP1 originally was to investigate if fatigue lifetimes could be prolonged by erasure of fatigue surface damage by corrosion at regular intervals. However, during a fatigue phase, cracks quickly initiated and grew past the surface layer affected by the next phase of corrosion. Thus, TP1 turned into an evaluation predominantly on the effect of accelerated corrosion on developed fatigue cracks. Section 2.2 describes test program 2 (TP2), where the effect of a single, eight-month period of natural corrosion in seawater on remaining lifetimes of fatigue-cracked specimens was investigated. The purpose of TP2 was to see if anodic dissolution would blunt the crack tip sufficiently to cause crack growth retardation. The design of the test programs allowed results for fatigue cracks at various stages of development to be obtained in a manageable time frame. It also provided some basis for comparison of natural and accelerated corrosion of fatigue cracks.

2. Methodology

2.1. TP1: Effect of periods of accelerated corrosion on fatigue lifetimes

In TP1, one group of precorroded specimens were fatigued to failure in air at room temperature. Fatigue tests on the other group of precorroded specimens were periodically interrupted, and the specimens underwent a phase of accelerated corrosion before fatiguing was resumed. This alternation was continued until failure, and the mean lifetimes of the two groups were compared. Specimens in the first and second group are hereafter referred to as *continuous fatigue* (CONT) and *alternating corrosion and fatigue* (ALT) specimens, respectively, even though they all underwent the same precorrosion phase.

Fatigue testing was done at high frequency in air. This was considered appropriate, since the dissolutive effect of corrosion on mooring chains is largest during the summer season. Corrosion was accelerated in order to complete several corrosion phases in a reasonably short time.

2.1.1. Specimen preparation

Notched specimens were cut from near the surface on the non-weld straight part of two connected ∅114 mm chain links made from R4-grade high-strength steel. The links had been laying on the deck of a floating production storage and offloading (FPSO) unit in the Norwegian Sea for 10 years. The links had minimal corrosion surface damage and had never experienced service loads. Figs. 1 and 2 show the cutting specification and machined specimen geometry. Yield strengths, $R_{p0.2}$, from position 5 of link 1 and 2 were measured to be 823 and 846 MPa, respectively. In both of the current test programs, it was assumed that any residual stresses from production of mooring chains [22,23] were relaxed during cutting of the specimens, and that any residual stresses that were introduced during machining were erased by material removal during the precorrosion phase.

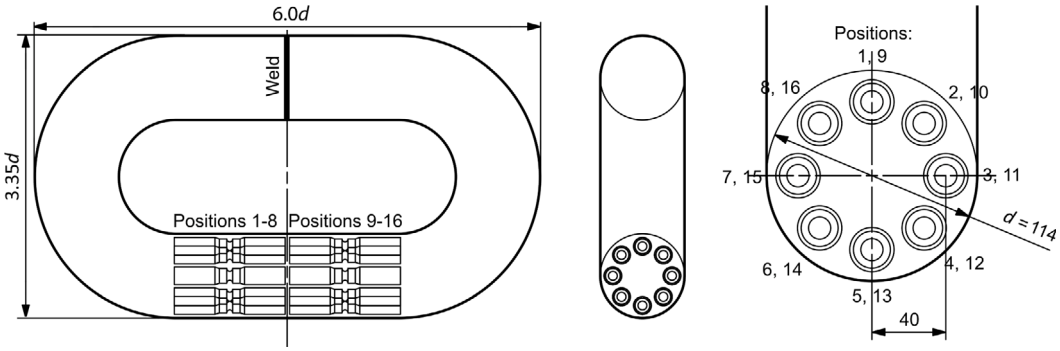

Fig. 1. Cutting specification for TP1 specimens from a chain link. All dimensions are given in millimeters.

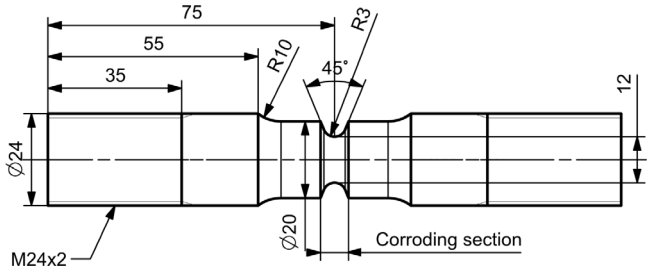

Fig. 2. As-machined specimen geometry for TP1. All dimensions are given in millimeters.

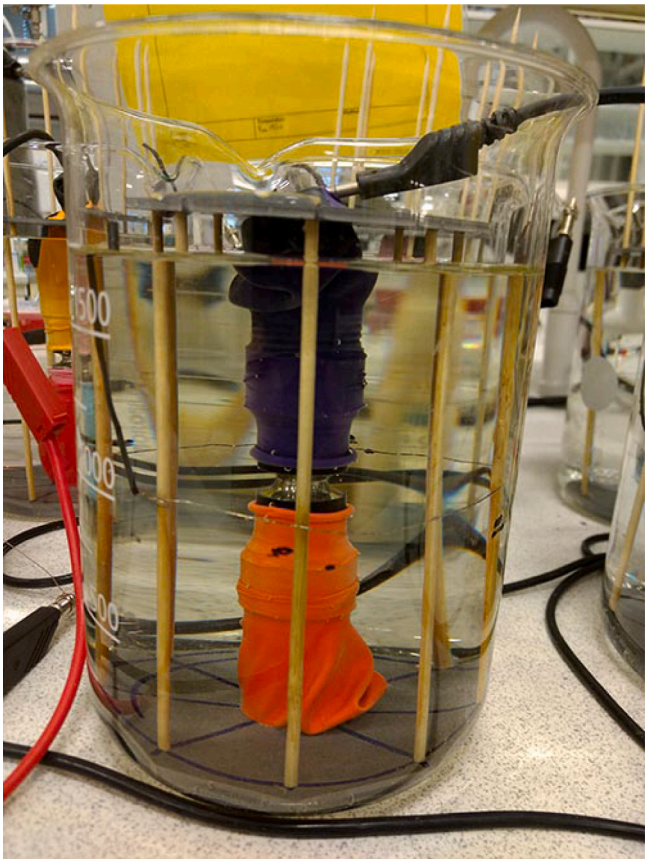

Fig. 3. Corrosion cell for anodic polarization of TP1 specimens during precorrosion and corrosion phases.

Fig. 4. Fatigue rig for tension loading in TP1. Housings of the spherical bearings that were installed to relieve any bending moment loads are visible.

2.1.2. Corrosion setup

The specimens were corroded in an unloaded state at room temperature in separate cells containing 3.5 wt% NaCl solution. All corrosion phases were accelerated by galvanostatic anodic polarization using a Gamry Interface 1000 galvanostat. The applied current density of 6.29×10^{-4} A/cm^2 was calculated [24] to give an average material removal rate of 20 μm/day across the corroding section of a specimen. The current density corresponds to a potential of about 100 mV above the open circuit potential [25]. The nominal surface area for application of current on the specimens was recalculated after the precorrosion phase. Platinum wire was used as cathode, arranged in a circular manner around each specimen, as shown in Fig. 3, to provide as uniform as possible current density in the notch surface on all sides. The non-corroding sections that are detailed in Fig. 2 were sealed off with tape. After each corrosion phase, any loose corrosion products were removed with a plastic brush, and the specimens were dried in warm air.

Precorrosion to remove 300 μm of material was carried out on all specimens to create a rough initial surface, and to limit the relative increase in roughness during subsequent corrosion phases. The corrosion phases on the ALT specimens were calculated to remove 100 μm of material per phase.

Corrosion rates of R4-grade and other carbon steels in seawater have been found to be 50–240 μm/year at temperatures below 18 °C [26,27]. The local corrosion rate on a chain link will depend on its location in a mooring line [28,29] and other factors. However, it can be concluded that 100 μm of average material removal by a corrosion phase is at least of the same order of magnitude as what can be expected on a chain from one summer season in service in the North or Norwegian Sea. The corresponding yearly corrosion rate on the specimens in the accelerated corrosion phases was 7.3 mm/year.

2.1.3. Fatigue setup

The specimens were fatigued in tension in an Instron 1603 electromagnetic resonance fatigue tester at a load frequency of about 170 Hz. Fig. 4 shows the fatigue rig. The load amplitude and ratio were 17 kN and 0.3, respectively. The load amplitude was calculated by finite element analysis (FEA) to correspond to a longitudinal stress amplitude in the notch after precorrosion of 281 MPa, when disregarding the stress raising effect from any corrosion pits. Details about all FEAs performed in the current work can be found in Appendix A. Fixings at both ends of the specimens had spherical bearings, to avoid any bending moment load on the specimens from misalignment. The temperature in the specimens during fatigue loading was not measured. Thus, no evaluation of the effect of temperature increase on fatigue lifetimes could be performed. For similar test programs in future research, this effect should be evaluated.

The tension fatigue setup and specimen geometry with a circular cross section and a relatively gentle notch was chosen to facilitate fatigue initiation in a limited segment of the specimen. This way, the development of fatigue damage or initiation in consistent locations on the circumference of the specimen could be followed during fatigue and corrosion phases. At the same time, the notch was not sharp enough to induce fatigue cracking immediately.

The CONT specimens (seven specimens) were fatigue tested until “failure”, i.e., full separation of the crack surfaces. Fatigue testing of the ALT specimens (eight specimens) was interrupted and corroded every 145,000 cycles (corresponding to about 46% of the recorded mean lifetime for the CONT specimens), in an attempt to conduct the corrosion phase before any large-scale crack growth had occurred. For clarity, the flowchart for TP1 is shown in Fig. 5.

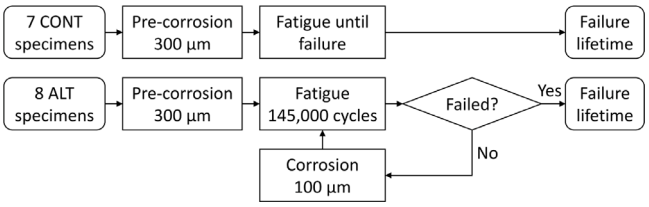

Fig. 5. Flowchart for TP1.

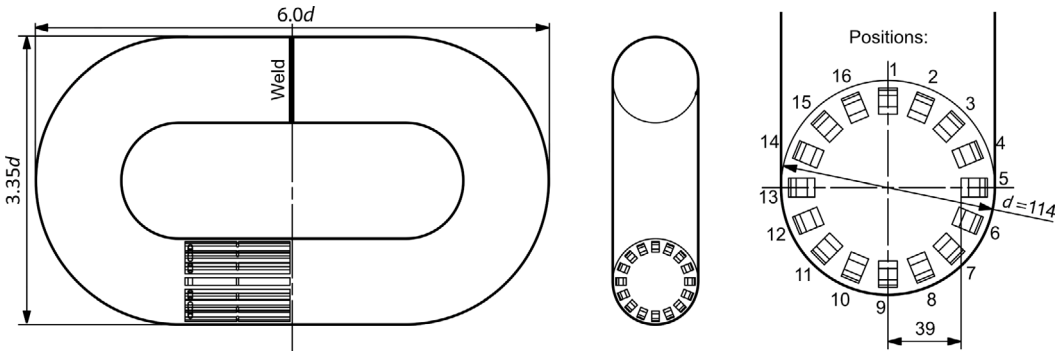

Fig. 6. Cutting specification from a chain link for the TP2 specimens. All dimensions are given in millimeters.

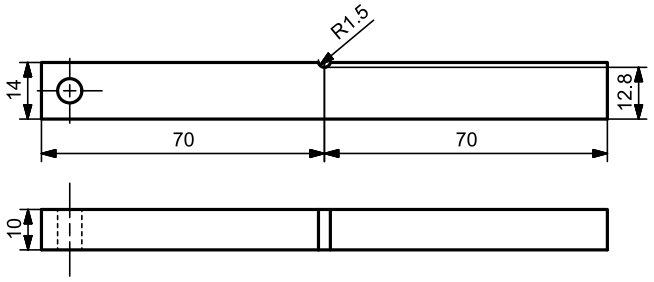

Fig. 7. As-machined specimen geometry for TP2. All dimensions are given in millimeters.

2.2. TP2: Effect of a period of natural corrosion on remaining lifetimes of fatigue-cracked specimens

For TP2, a group of *CONT* specimens were continuously fatigued to failure. A group of *ALT* specimens were fatigued until cracks of certain sizes had initiated. The ALT specimens were then left to corrode in seawater for eight months. Thereafter, fatiguing was resumed and continued until failure, and the remaining lifetimes were compared to that of the CONT specimens with similar crack sizes.

2.2.1. Specimen preparation

The TP2 specimens were designed for fatigue testing in a three-point bending setup. The reason for such a setup was that the bending stiffness of a specimen is sensitive to sizes of any cracks growing from the notch. This property was utilized to monitor crack growth, as described in detail in Section 2.2.3. Notched specimens were cut from the non-weld side of a link from the same chain as the specimens in TP1. Figs. 6 and 7 show the cutting specification and specimen geometry.

2.2.2. Corrosion setup

Precorrosion was carried out on all specimens, so that the ALT specimens, when cracked, could begin the subsequent corrosion phase with a homogeneously corroded surface free from residual machining stresses. The procedure and calculated average corrosion rate for the precorrosion phase was the same as in TP1, but only an average of 100 μm of material was removed. In the precorrosion cell, shown in Fig. 8, a platinum wire cathode was arranged at an even distance from the notch-side surface of the specimen to provide roughly uniform current density in the notch.

For the corrosion phase for the cracked ALT specimens, the specimens were left to corrode freely in seawater for 8 months, to allow the full effect of all time-dependent corrosion mechanisms in the fatigue cracks from a summer season. All specimens

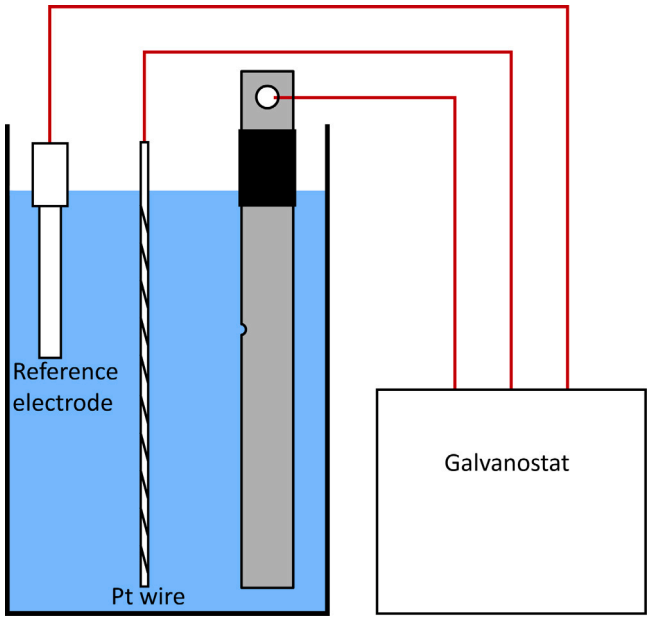

Fig. 8. Cell for precorrosion of a specimen in TP2. To accurately define the anode surface area on the specimen, the top of the specimen was sealed off with tape.

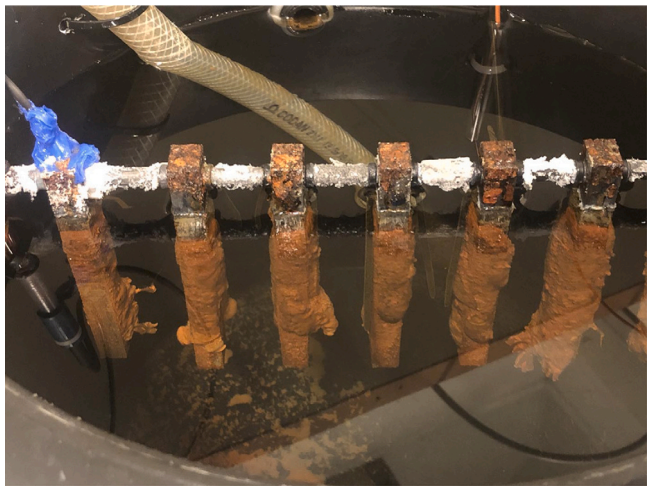

Fig. 9. Natural corrosion of the TP2 ALT specimens. Large amounts of oxide is visible.

were corroded together in a 15 l cell, shown in Fig. 9. Water was continuously pumped from 80 m depth in the Trondheim fjord (Trondheim, Norway) to an indoor laboratory. The flow rate through the corrosion cell was about 0.3 l/min. The water temperature varied between 10 and 16 °C. When the corrosion phase was finished, the specimens were cleaned with a plastic brush and dried.

2.2.3. Fatigue setup

The specimens were fatigued in three-point bending in an Amsler 100 HFP 5000 electromagnetic resonance fatigue tester at a load frequency of about 105 Hz. Fig. 10 shows a test specimen in the fatigue jig. Assuming that the degree of crack growth retardation from corrosion blunting might be sensitive to the load level, fatigue testing was done at two slightly different load levels, LL1 and LL2, as shown in Table 1. The loads were selected to give similar lifetimes as in TP1. Compared to in TP1, higher

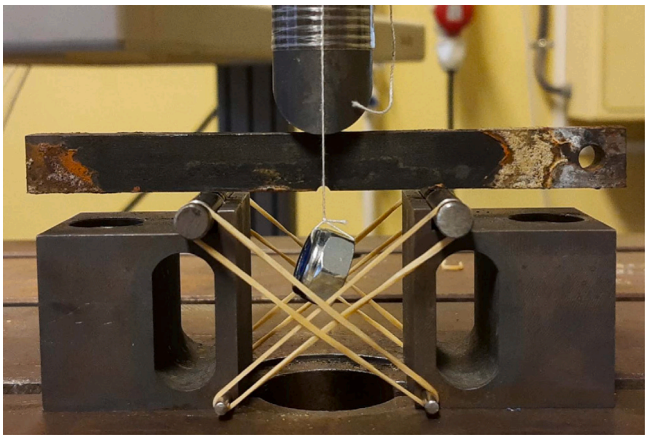

Fig. 10. TP2 three-point bending fatigue rig, with a distance between rollers of 56 mm. The nut and string are attached only for alignment purposes.

Table 1
Load level specifications. The longitudinal stress amplitude in the notch after precorrosion, calculated by FEA, is also stated.

Load level	Load amplitude/kN	Load ratio	Notch stress amplitude/MPa
LL1	3.30	0.3	397
LL2	3.47	0.3	418

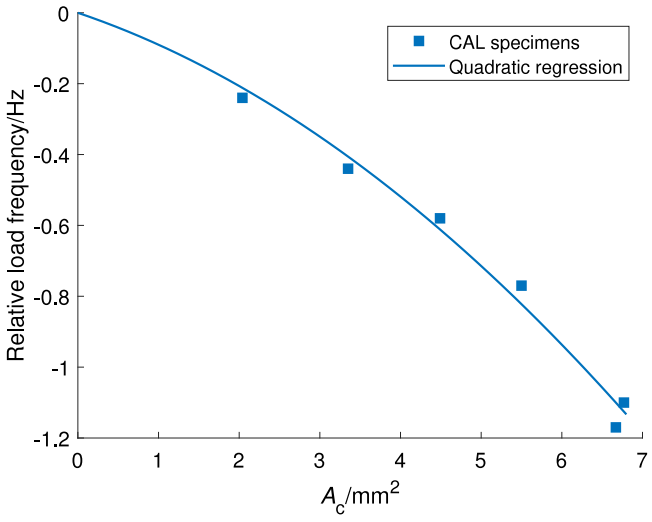

Fig. 11. Quadratic regression of relationship between total crack area and load frequency drop based on measurements on the CAL specimens.

surface stress amplitudes were needed. Reasons for this might be the less severe surface topographies on the specimens, due to a shorter precorrosion phase, or a steeper stress gradient due to the smaller notch and the applied bending load.

Before the CONT and ALT specimens were fatigued, a group of *calibration* (CAL) specimens were used to investigate the relationship between crack geometry and measured load frequency in the resonance fatigue tester. As a crack grows in a specimen, the bending stiffness of the specimen will be reduced. In a resonance fatigue tester, where the load frequency follows the natural frequency of the specimen and other vibrating components, this results in the load frequency dropping. In the current test program, the frequency drop was measured live and used to monitor crack growth. In order to translate the measured frequency drop into a useful crack geometry measurement, fatigue tests of six CAL specimens were stopped at different frequency drops of 0.2–1.2 Hz. The specimens were broken apart and the corresponding fatigue crack geometry was measured from the fracture surface. The 0.2 Hz value was chosen as the smallest frequency drop that could be detected over the noise of the load frequency signal. Such a detectable frequency drop indicated that a crack had initiated.

Fig. 11 shows the results of the calibration. A strong link between measured A_c, the total area of all cracks in a specimen, and frequency drops was registered. Quadratic regression resulted in a high coefficient of determination of $R^2 = 0.99$. Measured crack

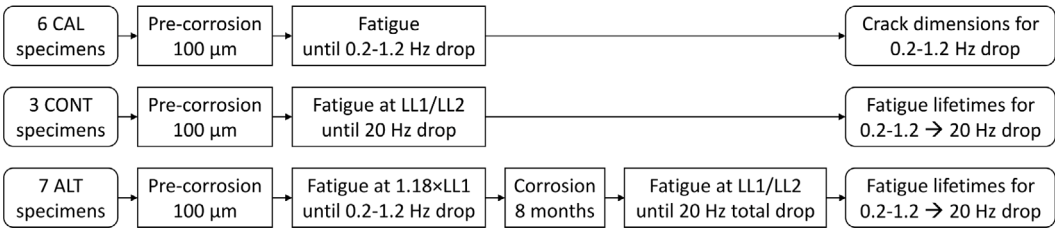

Fig. 12. Flowchart for TP2.

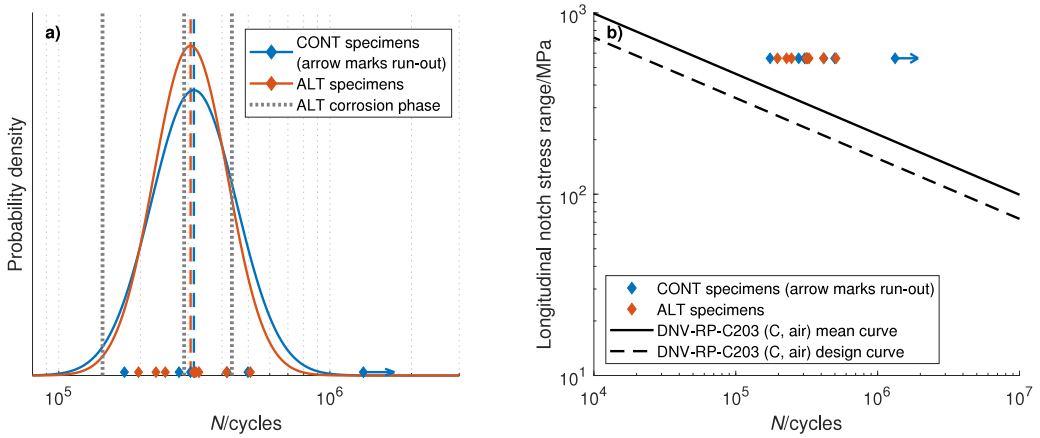

Fig. 13. (a) Probability density functions (solid lines) and mean $\log N$ (dashed lines) for both specimen groups. Diamond markers show observed lifetimes for individual specimens. (b) Comparison of the measured lifetimes with DNV-RP-C203 S–N mean and design (97.7% probability of survival) curves for detail category C in air.

depths showed a weaker correlation to the frequency drops than did the crack areas. Appendix C shows the fracture surfaces for the CAL specimens after they were broken off in liquid nitrogen. Details about crack geometries are provided in Appendix B.

From a theoretical point of view, it seems reasonable that a quadratic function would fit the data in Fig. 11 well. Derivations from the Euler–Lagrange equation for a freely vibrating, simply supported Euler–Bernoulli beam [30] with rectangular cross section yields a natural frequency, ω, that depends on the cross-section area to the power of 3/2 instead of 2, viz.

$$\omega \propto \sqrt{I} = \sqrt{\frac{wh^3}{12}} \propto A^{3/2}. \tag{1}$$

Here, I, w, h and A is the second moment of inertia, width, height and area of the beam cross section, respectively. However, this equation does not apply to notched and cracked specimens and does not include effects of vibrating parts of the fatigue tester.

After finishing the calibration, one CONT specimen was fatigued until failure at LL1, and two at LL2. The failure lifetime of a specimen was defined as the number of cycles for the load frequency to drop 20 Hz. This seemed to correspond to a crack covering nearly half of the original cross-section area of a specimen, see macrographs of the fracture surfaces in Appendix C. For the three specimens, the remaining lifetimes from measured frequency drops of 0.2–1.2 Hz until failure were noted and used as reference that the ALT specimens could be compared to.

Then, seven ALT specimens were fatigued until load frequency drops of 0.2–1.2 Hz. This was done at 18% higher load than LL1, to reduce the risk of any tests running out. The seven specimens were then corroded, before fatiguing was resumed and continued until the sum of frequency drops before and after corrosion was 20 Hz. Three specimens were fatigued at LL1, and four at LL2. The measured remaining lifetimes were compared to those of the CONT specimens at corresponding frequency drops and load levels. The flowchart for TP2 is shown in Fig. 12.

3. Results

3.1. TP1

Markers in Fig. 13a show the measured failure lifetimes, N, for all specimens. The results are also given in table form in Appendix B. Only one ALT specimen survived long enough to experience three corrosion phases (which are shown as gray, dotted lines every 145,000 cycles). Log-normal distributions have been fitted to both specimen groups by maximum likelihood

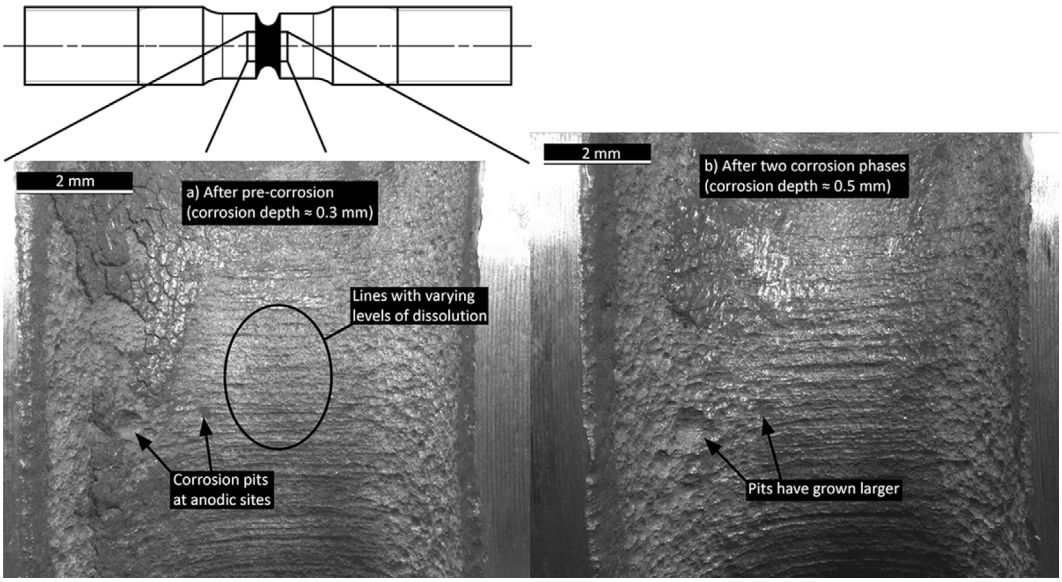

Fig. 14. Notch surface of an ALT specimen after a) precorrosion and b) two corrosion phases. Lines parallel to the rolling direction at the notch base likely results from microstructural features of former, elongated austenite grains.

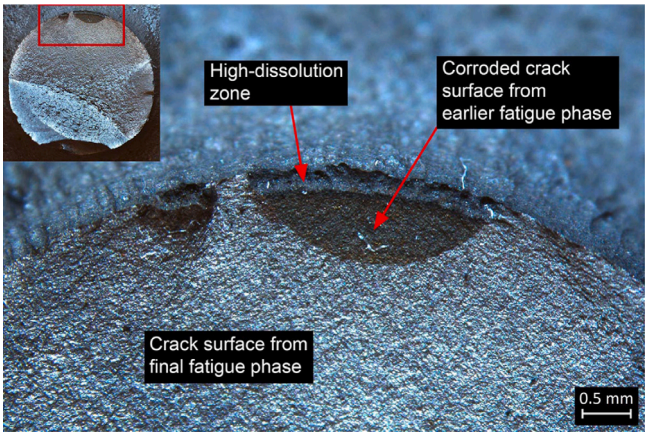

Fig. 15. Appearance of corroded cracks on the fracture surface of an ALT specimen after a corrosion phase and subsequent fatiguing.

regression [31]. Solid lines show the probability density functions (PDFs). For reference to offshore standards, the measured lifetimes have been plotted together with S–N curves from DNV-RP-C203 [32] in Fig. 13b.

The one CONT specimen that endured several times more load cycles than any other CONT specimens has been considered an outlier and disregarded during fitting of the PDF. Moreover, this specimen failed due to fatigue in threads, and the test is therefore marked as a run-out. During the test, the load frequency started dropping already at around 1.08×10^6 cycles, indicating a growing crack in the threads and, thus, possibly an altered stress distribution in the notch.

Even though the measured $\log N$ for the ALT specimens (mean = 5.49, standard deviation = 0.14) were on average slightly lower than for the continuous fatigue specimens (mean = 5.50, standard deviation = 0.16), an independent-samples t-test revealed that the difference was not significant, $t(12) = 0.15$, $p = 0.44$.

Fig. 14 shows macrographs of the notch surface of an ALT specimen after a) precorrosion and b) two corrosion phases. Since corrosion was accelerated by anodic polarization, one can imagine that shorter distances between protruding surface features and the cathode may have resulted in decreased electrolyte resistance and higher current densities at these, thus causing some degree of surface leveling. Nevertheless, the resulting surfaces in Fig. 14 are relatively rough, with obvious anodic and cathodic sites. By the end of the second corrosion phase, it is apparent that the surface has evolved into a slightly rougher one, and pits at persistent anodic sites have increased in size. The larger pits might have led to higher stresses at and near the surface, promoting earlier fatigue crack initiation than if the surface had remained in the precorroded state.

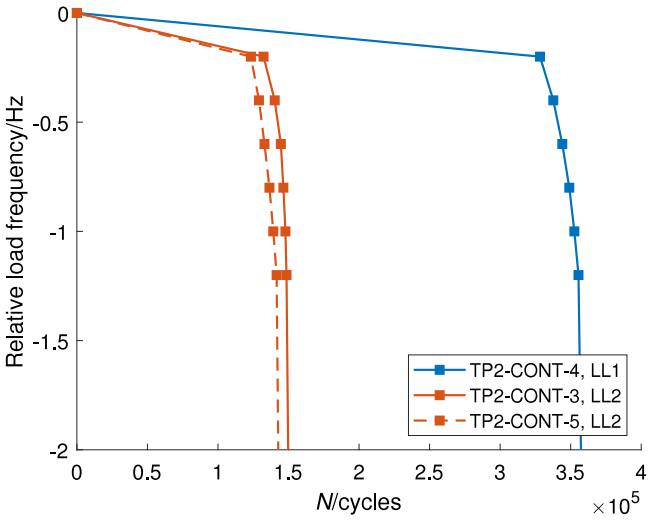

Fig. 16. Cycle count measurements at different load frequency drops for the CONT specimens. Each line represents one specimen, with IDs corresponding to the notation from Appendix B.

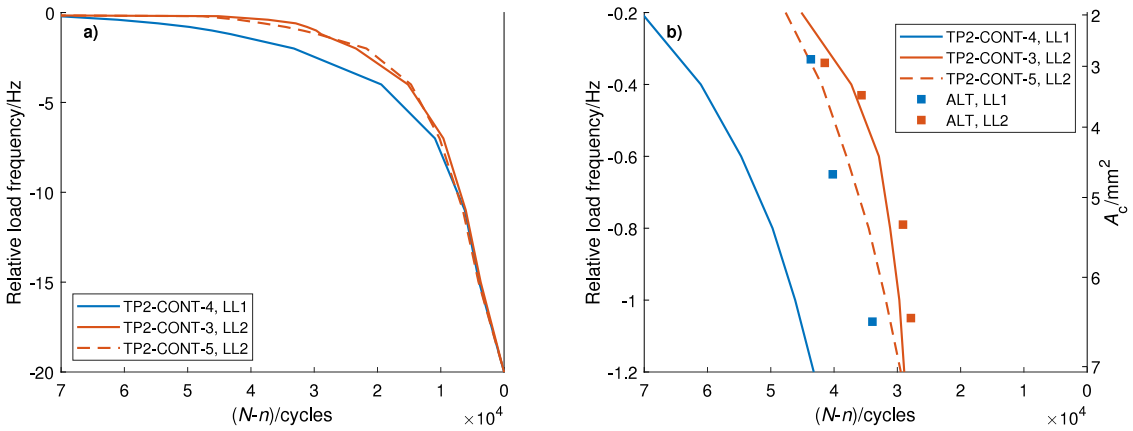

Fig. 17. (a) Remaining lifetime of the cracked CONT specimens at different load frequency drops. (b) Comparison with the cracked ALT specimens after eight months of corrosion and fatigue testing until failure.

From Fig. 15, which shows cracks in an ALT specimen after a corrosion phase, it can be seen that the dissolution rate has been high along the crack mouth down to a depth of about 0.2 mm during the anodic polarization. This indicates an anodic site for large cracks that is not at the crack tip, at which the dissolutive effect of corrosion might thus be limited.

From fractographs in Appendix C, it seems that all ALT specimens failed by fracture from cracks that had corroded in the previous corrosion phase. Of three specimens with corroded cracks that were shallow enough to be enclosed by the aforementioned zone of high dissolution, only one specimen experienced more than one corrosion phase. For the other two, it is thus clear that the extensive blunting of the crack tip did not retard crack growth sufficiently for the specimen to survive until the next corrosion phase. Four ALT specimens with larger corroded cracks showed even bands of high dissolution along the crack mouths, which indicated that the crack surfaces had been exposed only during the last corrosion phase.

3.2. TP2

Fig. 16 shows the load frequency drop measurements that were done on the CONT specimens at different cycle counts, n. In Fig. 17a, the curves from Fig. 16 have been translated horizontally so that the failure lifetimes (N) of the three specimens are aligned on the right vertical axis. By normalizing the curves by failure lifetime, the remaining lifetime, $N - n$, of a specimen at a

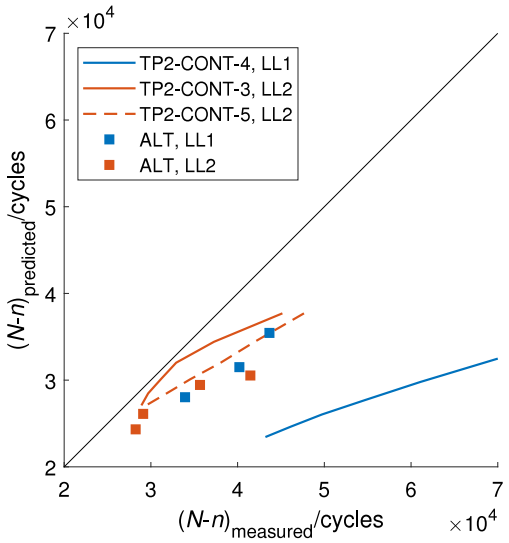

Fig. 18. Remaining lifetimes predicted according to BS 7910, compared to measured remaining lifetimes.

certain frequency drop can be read from the horizontal axis. In the current work, the remaining lifetime (consisting of crack growth) was adopted as measure for comparing lifetimes of the CONT and ALT specimens, to avoid the higher scatter often associated with crack initiation times.

In Fig. 17b, remaining lifetimes that were measured for the ALT specimens after the corrosion phase have been plotted by markers, for comparison with the CONT specimen curves. The right axis shows the crack areas that correspond to the load frequency drops on the left axis, as calculated from the quadratic-regression fit of Fig. 11. For LL2, there seem to be not much deviation between the CONT and the ALT specimens. For LL1, remaining lifetimes of the ALT specimens are slightly longer than for LL2, as expected. However, the remaining lifetime of the single CONT specimen is much longer than those of the corresponding ALT specimens.

To provide additional background for discussion, remaining lifetimes of the CONT and ALT specimens were predicted based on the crack growth rates of ferritic steel in air given in the BS 7910 standard [33]. The crack growth calculations were carried out by using a SIF solution for a single-edge-cracked bending specimen with rectangular cross section [34], while assuming an initial crack depth of $a = d + A_c/W$. Here, d and W is the notch depth and specimen width, respectively. While this approach might be crude, it allows for some degree of comparison between the CONT and ALT specimens. Fig. 18 shows the calculation results together with measured remaining lifetimes. It can be seen that, although the calculations slightly underestimate the measurements, the scatter is relatively low. The exception is the CONT specimen loaded at LL1, for which the measured remaining lifetimes are far higher than predicted. Reasons for this will be discussed later in the succeeding section.

4. Discussion

Contrary to what was expected, the corrosion phases did not have any significant effects on remaining fatigue lifetimes in air. Some likely explanations for this observation are given here, as well as what can be inferred from this finding regarding fatigue of mooring chains.

Firstly, the method for accelerating the corrosion phases in TP1 is reviewed. TP1 was designed to explore the effect of corrosion on fatigue surface damage. However, cracks initiated and developed too quickly to highlight this topic extensively. Thus, the relevant site for corrosion shifted to the crack tip, where the corrosion mechanisms are geometrically more restricted. Since the electrolyte resistance is inversely proportional to the area through which charge is being carried, the narrow opening of a fatigue crack results in a very high resistance, thus limiting the current. Therefore, after a fatigue crack had initiated in a specimen, the effect of accelerating corrosion with the current method was likely very limited at the crack tip.

Significant effects of the corrosion phases can thus only be expected for fatigue surface damage and for short cracks in the high-dissolution zone. By the looks from the notch surface outside a corroded crack in a dummy specimen in Fig. 19, it seems that the crack's width of around 0.2 mm in the high-dissolution zone is at least as extensive as could be expected from average corrosion rates in the North Sea. Yet, for the shallow, corroded cracks from TP1, it has been shown that corrosion did not seem to have a great lifetime-extending effect from crack tip blunting.

As no high-dissolution zone is visible on the corroded crack surfaces of TP2, the current way of accelerating corrosion exhibits dissolutive patterns in cracks that are clearly deviating from those in naturally corroding cracks. Thus, when studying corrosion effects on cracks, specimens should be subjected to natural corrosion to obtain the most accurate results.

For determining effects of corrosion phases on fatigue cracks in TP2, the remaining lifetimes of CONT and ALT specimens were compared. It was assumed that the crack growth is a relatively deterministic phenomenon, and that the crack growth rate depends

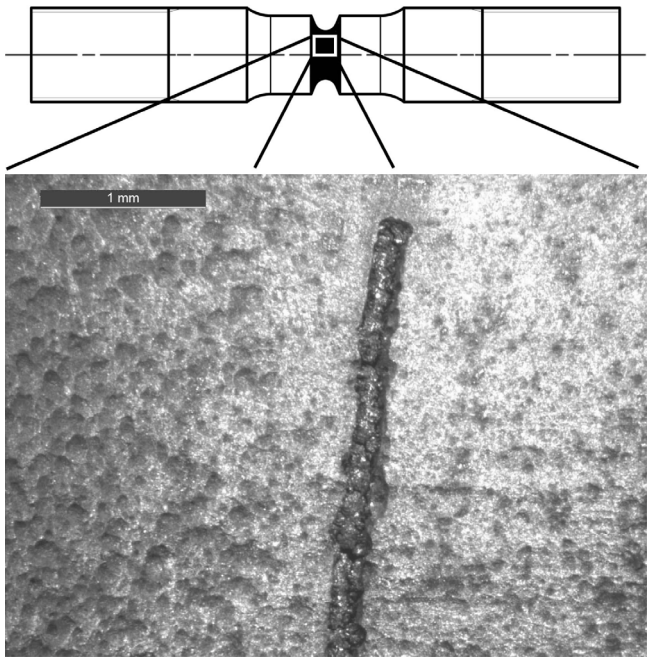

Fig. 19. Corroded crack in the notch of a dummy specimen in TP1.

closely on the crack driving force. Thus, two specimens with similar geometry and crack shape should have roughly the same remaining lifetime if loaded equally under the same conditions. However, even if two cracks yielded the same load frequency drop in fatigue tests, indicating similar crack areas, it does not mean that their shape is the same. Thus, the SIF ranges may differ between the cracks, and so will the crack growth rate. The CONT specimen that was subjected to LL1 is shown in Fig. 17 to have considerably longer remaining lifetime than the specimens subjected to LL2 have, at only 5% lower load. This seems peculiar and might have been a result of an atypical crack shape in the specimen and a less critical SIF range at the crack tip. Even though there was scatter in the rest of the TP2 results, it seemed to be low enough in the results from both CONT and ALT specimens to conclude that the eight-month corrosion phase at least did not have a large impact on the state of the cracks of the ALT specimens.

To explain this insensitivity to the corrosion phase, some discussion on the hypothesis that blunting of a crack by corrosion can retard crack growth is useful. As already mentioned, several authors have found that a corrosion pit has an equally severe SIF as a crack of the same depth [10,15,16]. It can be argued that a crack blunted by corrosion cannot have a geometry that is less stress-raising than a corrosion pit. Thus, it seems unlikely that blunting by corrosion would have a significantly retarding effect on crack growth. Any retarding effects that might be observed, are assumed to be results of other mechanisms. A mechanical explanation may be that even if a crack appears “blunted”, the crack tip is not smooth. There may exist severe microscopic surface features that facilitates swift crack reinitiation. Even macroscopically, a blunted crack is still a very powerful local stress raiser, which too promotes crack reinitiation.

In the current test programs, the intensity and duration of the load in a fatigue phase might have deviated from what a mooring chain experiences during a winter storm. On small-scale fatigue tests of corroded surfaces of offshore mooring chains under high loads, fatigue initiation times have been demonstrated to be relatively short [35]. If, because of higher loads, initiation times in the current tests are shorter than for chains in service, then the potential for fatigue process retardation is reduced. Work is under way to quantify the magnitudes of the stresses in mooring chains in service, so that the relevance of the current tests can be evaluated.

Whereas mooring chains are subjected to stochastic loading and continuous corrosion, the test conditions in the current work were simplified by separating the corrosion and fatigue phases. In both phases, the simplification likely leads to reduced dissolution at the crack tip from corrosion compared to in-service conditions: In the summer season, static stresses from pretensioning and self-weight loads on an offshore mooring chain would increase crack opening and crack tip strains, promoting higher dissolution rates. In winter, the presence of seawater during load cycling would also lead to some additional dissolution. However, even though these effects would result in more pronounced crack tip blunting, the arguments about its effects on fatigue behavior still apply, and it is unlikely that blunting significantly retard further crack growth.

The absence of the corrosive environment during the fatigue phases is furthermore likely to push lifetime results in a non-conservative way compared to in-service conditions for mooring chains. Nevertheless, applying alternating corrosion and fatigue phases is seen as a practical way of investigating qualitative effects on crack development of the relevant seasonal extreme load variations during corrosion fatigue.

In order to stay within the load limitations of the fatigue rig used in TP1, specimen dimensions had to be kept relatively small. Consequently, as a result of reducing the specimen cross sections with each corrosion phase, the surface stresses in the notch grew.

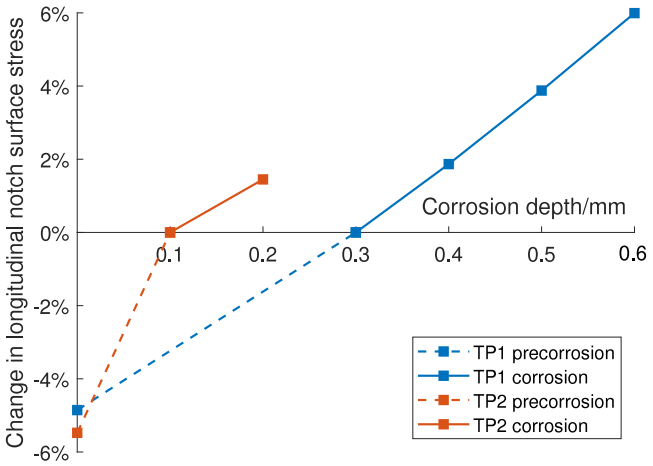

Fig. 20. Longitudinal notch surface stresses calculated by FEA after removal of material layers with uniform depths. The depths of the removal of material are corresponding to estimated removed material from corrosion phases. The stresses have been normalized w.r.t. the stresses after precorrosion.

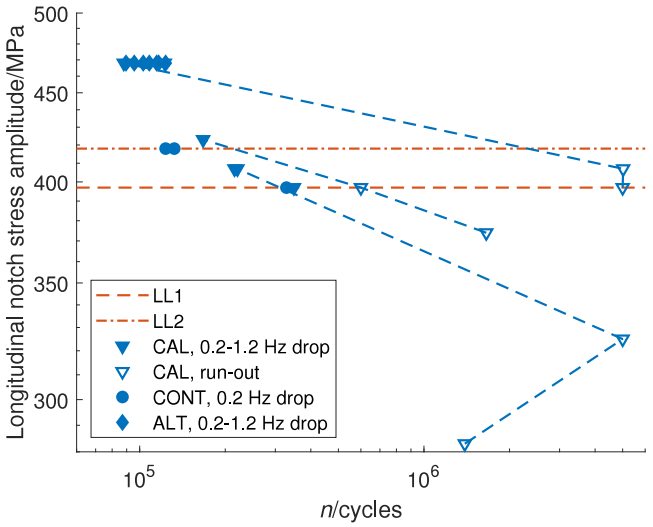

Fig. 21. Surface stress amplitude *S-N* plot of all specimens from the first fatigue phase of TP2. For the CONT specimens, the cycle count until 0.2 Hz load frequency drop is shown. Unfilled markers show run-outs, and dashed lines connect measurements that were made on the same specimen.

An increasing notch radius also meant that the stress-raising effect of the notch extended deeper into the material. These increased stresses, in addition to raised surface stresses from growing corrosion pits, promoted faster crack initiation. To yield conservative results, no adjustments were made to the load during the course of the testing. Thus, in order to limit the increase of stresses in the notch, corrosion phases had to happen relatively infrequently. Fig. 20 shows the nominal effect on the notch surface stresses from the corrosion phases, calculated by FEA, assuming uniform material removal rates. For the specimen that underwent three corrosion phases, a final change in stress of 6.0% was calculated. This might have had a substantial impact on the total fatigue lifetime.

For TP2, the effect was less pronounced, with notch stresses for the ALT specimens being only 1.4% higher after the corrosion phase, assuming that 0.1 mm of material was removed uniformly across the surface during this phase.

Because of the larger dimensions of mooring chains, the same material removal rates as used in these tests will, of course, have less effect on chain surface stresses than in the specimens.

To give the reader a sense of the stress levels used in TP2, measured cycle counts for the first fatigue phase of all TP2 specimens have been compiled in S–N format in Fig. 21. This means, for the CAL specimens, all cycles until they were cracked open in liquid

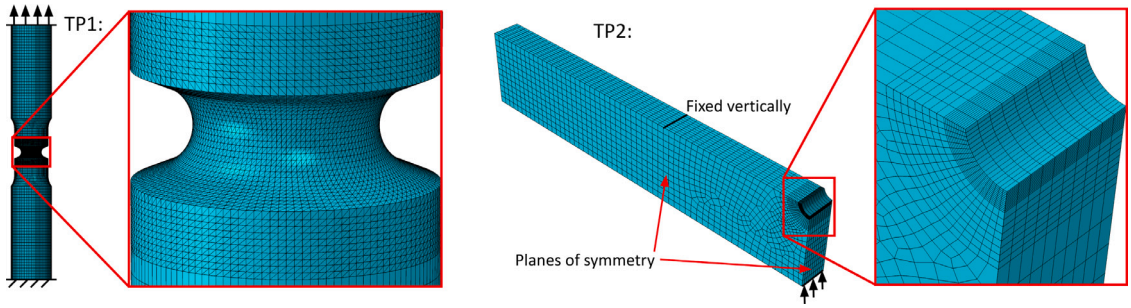

Fig. A.22. FEA models used in the current work.

Table B.2
TP1 specimen positions and measured lifetimes. Positions refer to Fig. 1.

Specimen ID	Link ID	Position on link	N/cycles	No. of corrosion phases (after precorrosion)
TP1-CONT-1-1	1	1	417,758	N/A
TP1-CONT-1-12	1	12	498,589	N/A
TP1-CONT-1-14	1	14	306,174	N/A
TP1-CONT-2-4	2	4	1,328,576[a]	N/A
TP1-CONT-2-6	2	6	316,096	N/A
TP1-CONT-2-8	2	8	174,610	N/A
TP1-CONT-2-14	2	14	277,691	N/A
TP1-ALT-1-5	1	5	509,112	3
TP1-ALT-1-6	1	6	313,607	2
TP1-ALT-1-9	1	9	196,800	1
TP1-ALT-1-10	1	10	320,370	2
TP1-ALT-1-15	1	15	247,110	1
TP1-ALT-2-5	2	5	415,814	2
TP1-ALT-2-12	2	12	228,170	1
TP1-ALT-2-15	2	15	328,721	2

[a]Run-out because of failure in the threads.

nitrogen. For the CONT specimens, the cycles until 0.2 Hz frequency drop are shown, and for the ALT specimens, the cycles endured at load 18% above LL1. Surface stress amplitudes have been calculated by FEA. The load levels in TP2 were chosen by means of gradually stepping up the load for a few run-out CAL specimens until load frequency drops could be observed. In the figure, results from the step-up of load have also been included. All markers connected by dashed lines represent the same specimen. From the large scatter at medium loads, it may seem that the final testing loads are just above the fatigue limit — or at least a lifetime regime governed by a gentler-slope S–N curve.

5. Conclusions

In the current study, two test programs of alternating corrosion and fatigue phases on R4-grade steel were conducted to replicate seasonal load variations on offshore mooring chains in service. One was on the effect of periodic phases of corrosion on fatigue lifetime of precorroded specimens. Here, corrosion was accelerated by anodic polarization. The other was on the effect of eight months of natural corrosion on the remaining lifetime of specimens with fatigue cracks.

For the specimens in the first test program, no significant difference in mean lifetime was registered compared to the reference group that was fatigued in air. Extensive blunting of shallow fatigue cracks in a few specimens did not seem to retard further crack growth to a large degree. However, in the majority of the specimens, cracks grew deep during fatigue phases, largely restricting any effect from accelerated corrosion processes at the crack tip during the following corrosion phase. Thus, accelerated corrosion is deemed unsuitable for studies of effects of natural corrosion on cracks. A weakness in the current test setup was that surface stresses were increased with each corrosion phase, promoting faster crack initiation in the specimens undergoing corrosion phases than in the reference group.

In the second test program, contrary to what was expected, no large extending effect on remaining lifetimes from crack tip blunting by natural corrosion was registered. However, the conclusion that a fatigue crack blunted by corrosion is as critical as a sharp one is supported by observations in the literature. This implies that any potentially retarding effects on crack growth likely result from other mechanisms.

Table B.3
TP2 specimen positions, load levels and measured crack sizes and lifetimes. Positions refer to Fig. 6.

Specimen ID	Position on link	Load level	A_c/mm^2	Depth of deepest crack/mm	Frequency drop before corrosion/Hz	N/cycles	$(N-n)$/cycles
TP2-CAL-6	6	1.18 × LL1	6.77	1.1	−1.1	122,515	N/A
TP2-CAL-8	8	1.07 × LL1[a]	3.35	1.19	−0.44	167,147	N/A
TP2-CAL-11	11	1.03 × LL1	5.5	1.58	−0.77	215,515	N/A
TP2-CAL-12	12	1.18 × LL1[a]	2.04	0.71	−0.24	87,903	N/A
TP2-CAL-15	15	1.03 × LL1[a]	6.67	1.47	−1.17	220,686	N/A
TP2-CAL-16	16	LL1	4.49	1.34	−0.58	348,815	N/A
TP2-CONT-3	3	LL2	N/A	N/A	−20	175,598	N/A
TP2-CONT-4	4	LL1	N/A	N/A	−20	396,688	N/A
TP2-CONT-5	5	LL2	N/A	N/A	−20	168,905	N/A
TP2-ALT-1	1	LL2	N/A	N/A	−0.34	95,700	41,470
TP2-ALT-2	2	LL2	N/A	N/A	−0.43	89,503	35,664
TP2-ALT-7	7	LL2	N/A	N/A	−0.79	114,790	29,110
TP2-ALT-9	9	LL2	N/A	N/A	−1.05	108,092	28,243
TP2-ALT-10	10	LL1	N/A	N/A	−1.06	116,604	33,940
TP2-ALT-13	13	LL1	N/A	N/A	−0.33	102,938	43,670
TP2-ALT-14	14	LL1	N/A	N/A	−0.65	123,372	40,203

[a]Last applied load level. Specimens also sustained significant numbers of cycles at lower load levels. See Fig. 21 for details.

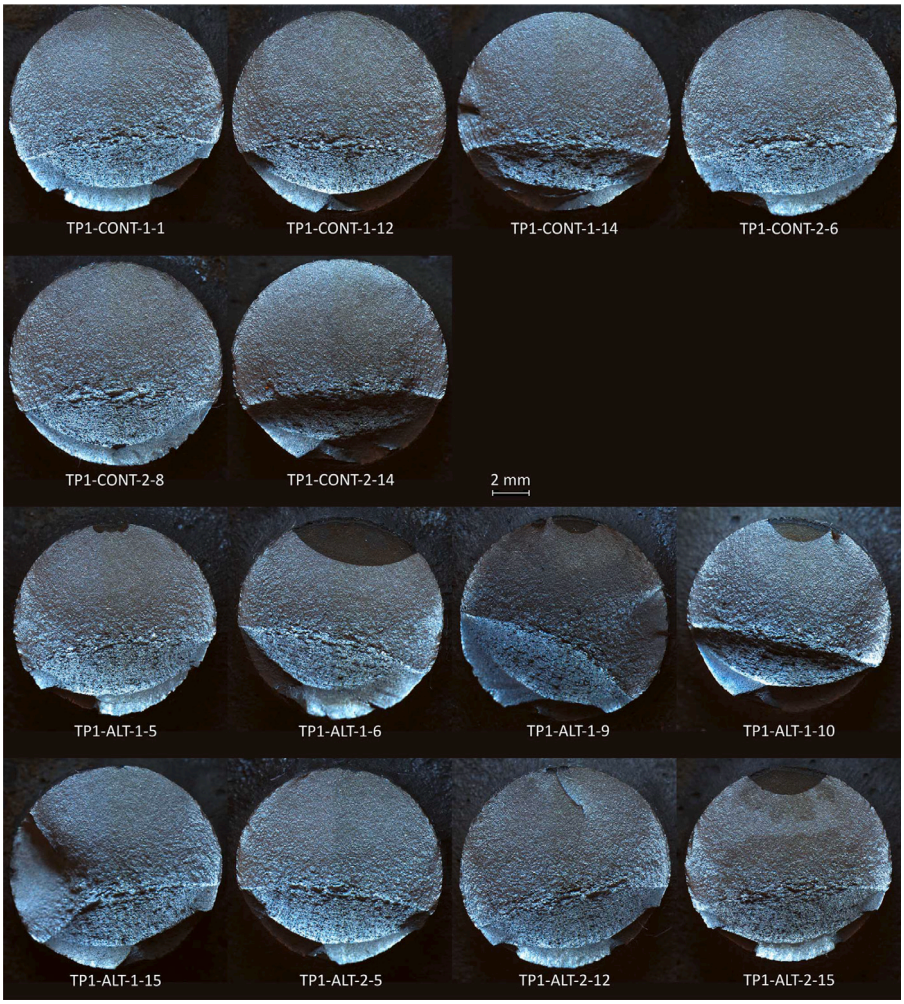

Fig. C.23. Macrographs of fracture surfaces of specimens from TP1. Codes on the figure refer to the specimen IDs stated in Table B.2.

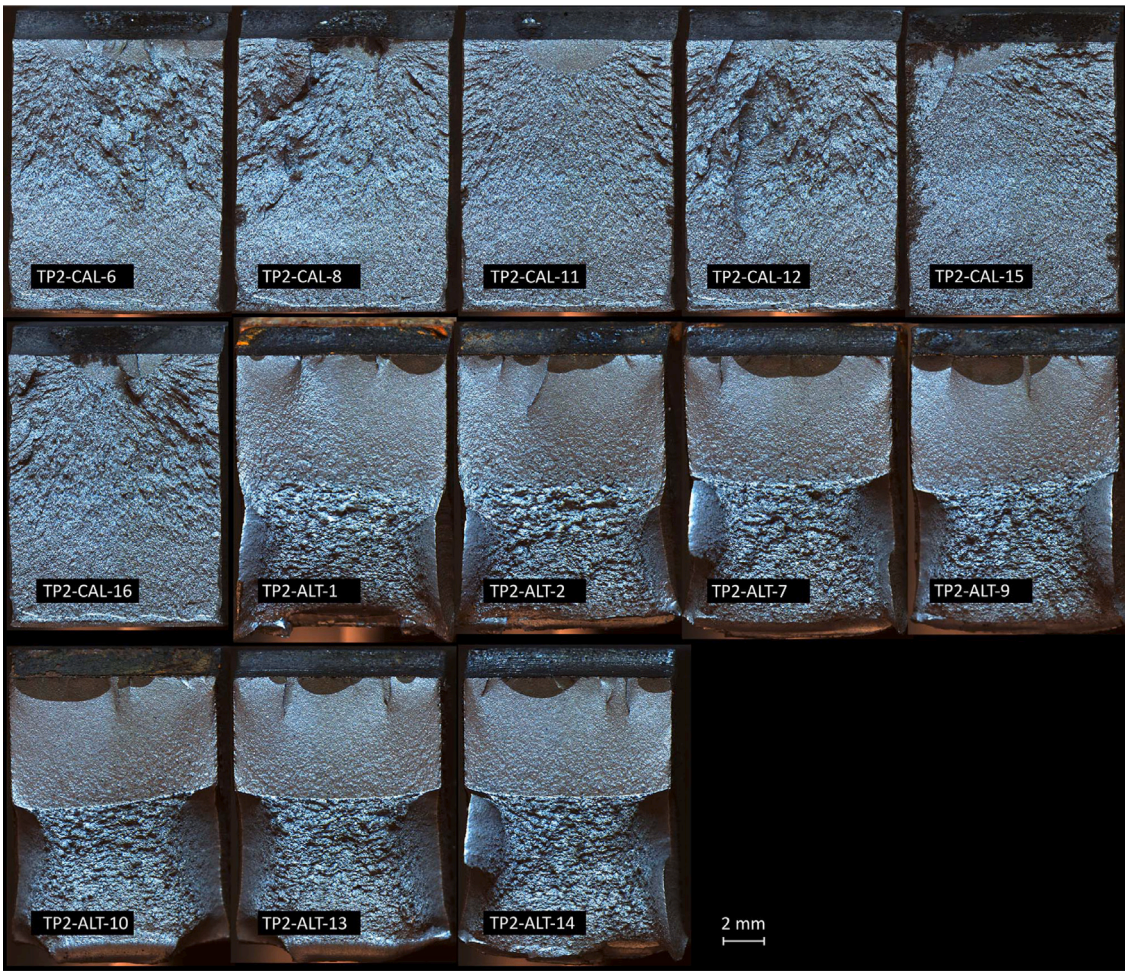

Fig. C.24. Macrographs of fracture surfaces of specimens from TP1. Codes on the figure refer to the specimen IDs stated in Table B.3. The CAL specimens were submerged in liquid nitrogen and cracked open after fatiguing to different crack depths. The ALT specimens were cracked open in ambient temperature after fatiguing until 20 Hz load frequency drop. Fracture surfaces of some CAL specimens were damaged by corrosion in air during storage. Specimens TP2-ALT-1 and TP2-ALT-2 were fatigued until unstable fracture at load frequency drops between 20 and 25 Hz, instead of terminating the fatiguing at 20 Hz drop. However, the cycle count at 20 Hz drop was used for lifetime evaluations.

Declaration of competing interest

The authors declare that they have no known competing financial interests or personal relationships that could have appeared to influence the work reported in this paper.

Acknowledgments

The authors would like to thank O. ∅. Knudsen, A. Erbe, T. A. Kristensen, A. Hellesvik, M. Aursand, C. Torres and other researchers and staff at SINTEF and NTNU for helpful discussions on the experimental setup and results processing. This work was supported through the project KPN LifeMoor by the Research Council of Norway (RCN contract no.: 280705).

Appendix A. FEA methodology

All FEAs in the current work was performed using the Abaqus 2017 software and 3D solid models. Material properties for R4-grade steel was implemented in the form of a monotonic material model from [36].

The meshed FEA models are shown in Fig. A.22. For TP1, the whole specimen was modeled. As boundary condition, one end surface of the specimen was fixed. The axial load was applied on the other end surface, while forcing this surface to remain plane. Quadratic-order tetrahedron elements (C3D10) was used in and around the notch. The element length was 0.39 mm in the tangential direction of the notch. Thus, each element covered a 7° sector of the notch profile. The total element count in the model was 332,730.

In TP2, the two planes of symmetry were utilized to model only one quarter of a specimen. In the location of the support rollers (see Fig. 10), vertical translations were fixed. The load was applied along a non-deformable line at the center of the specimen, representing the load punch. Linear-order hexahedron elements (C3D8) were used in the model. The element length in tangential direction of the notch was 0.11 mm, covering 4° of the notch profile. The total element count was 12,090.

For calculating stresses after corrosion phases, specimen dimensions were changed accordingly, and the models were remeshed.

Appendix B. Specimen details and lifetimes

See Tables B.2 and B.3.

Appendix C. Macrographs of fracture surfaces

See Figs. C.23 and C.24.

References

[1] Fernández J, Storesund W, Navas J. Fatigue performance of grade R4 and R5 mooring chains in seawater. In: Proceedings of the ASME 2014 33rd International Conference on Ocean, Offshore and Arctic Engineering. ASME; 2014, http://dx.doi.org/10.1115/OMAE2014-23491.

[2] Lone EN, Sauder T, Larsen K, Leira BJ. Probabilistic fatigue model for design and life extension of mooring chains, including mean load and corrosion effects. Ocean Eng 2022;245:110396. http://dx.doi.org/10.1016/j.oceaneng.2021.110396.

[3] Bauer E. Interannual changes of the ocean wave variability in the North Atlantic and in the North Sea. Clim Res 2001;18(1–2):63–9. http://dx.doi.org/10.3354/cr018063.

[4] Gabrielsen Ø, Liengen T, Molid S. Microbiologically influenced corrosion on seabed chain in the North Sea. In: Proceedings of the ASME 2018 37th International Conference on Ocean, Offshore and Arctic Engineering, Vol. 3. ASME; 2018, http://dx.doi.org/10.1115/OMAE2018-77460.

[5] Ma K, Gabrielsen Ø, Li Z, Baker D, Yao A, Vargas P, et al. Fatigue tests on corroded mooring chains retrieved from various fields in offshore West Africa and the North Sea. In: Proceedings of the ASME 2019 38th International Conference on Ocean, Offshore and Arctic Engineering, Vol. 3. ASME; 2019, http://dx.doi.org/10.1115/OMAE2019-95618.

[6] Schijve J. Fatigue of Structures and Materials. 2nd ed.. Springer Netherlands; 2009, http://dx.doi.org/10.1007/978-1-4020-6808-9.

[7] Gangloff RP. Corrosion fatigue crack propagation in metals. In: 1st International Conference on Environment Induced Cracking of Metals. NASA; 1990, URL https://ntrs.nasa.gov/citations/19900015089.

[8] Shipilov SA. Mechanisms for corrosion fatigue crack propagation. Fatigue Fract Eng Mater Struct 2002;25(3):243–59. http://dx.doi.org/10.1046/j.1460-2695.2002.00447.x.

[9] Suresh S, Ritchie R. Near-threshold fatigue crack propagation: A perspective on the role of crack closure. Tech. rep, Lawrence Berkeley National Laboratory; 1983, LBL-16263 URL https://escholarship.org/uc/item/8mr83283.

[10] Komai K, Minoshima K, Kinoshita S, Kim G. Corrosion fatigue crack initiation of high-tensile-strength steels in synthetic seawater. JSME Int J Ser 1, Solid Mech Strength Mater 1988;31(3):606–12. http://dx.doi.org/10.1299/jsmea1988.31.3_606.

[11] Austen I. Quantitative assessment of corrosion fatigue crack growth under variable amplitude loading. Tech. rep, London, UK: British Steel Corporation; 1988.

[12] Radon JC, Branco CM, Culver LE. Crack blunting and arrest in corrosion fatigue of mild steel. Int J Fract 1976;12(3):467–9. http://dx.doi.org/10.1007/BF00032842.

[13] Menan F, Henaff G. Influence of frequency and exposure to a saline solution on the corrosion fatigue crack growth behavior of the aluminum alloy 2024. Int J Fatigue 2009;31(11):1684–95. http://dx.doi.org/10.1016/j.ijfatigue.2009.02.033, Fatigue Damage of Structural Materials VII.

[14] Yamamoto N, Sugimoto T, Ishibashi K. Fatigue strength assessment of a structure considering corrosion wastage and corrosion fatigue. In: Proceedings of the ASME 2018 37th International Conference on Ocean, Offshore and Arctic Engineering, Vol. 3. ASME; 2018, http://dx.doi.org/10.1115/OMAE2018-78188.

[15] Kondo Y. Prediction of fatigue crack initiation life based on pit growth. Corrosion 1989;45(1):7–11. http://dx.doi.org/10.5006/1.3577891.

[16] Ishihara S, Saka S, Nan Z, Goshima T, Sunada S. Prediction of corrosion fatigue lives of aluminium alloy on the basis of corrosion pit growth law. Fatigue Fract Eng Mater Struct 2006;29(6):472–80. http://dx.doi.org/10.1111/j.1460-2695.2006.01018.x.

[17] Montgomery EL, Calle LM, Curran JC, Kolody MR. Timescale correlation between marine atmospheric exposure and accelerated corrosion testing – part 2. In: Corrosion 2012. NACE; 2012, NACE-2012-1730 URL https://onepetro.org/NACECORR/proceedings/CORR12/All-CORR12/NACE-2012-1730/120250.

[18] Baldwin K, Smith C. Accelerated corrosion tests for aerospace materials: Current limitations and future trend. Aircr Eng Aerosp Technol 1999;71(3):239–44. http://dx.doi.org/10.1108/00022669910270718.

[19] Du M, Chiang F, Kagwade S, Clayton C. Damage of Al 2024 alloy due to sequential exposure to fatigue, corrosion and fatigue. Int J Fatigue 1998;20(10):743–8. http://dx.doi.org/10.1016/S0142-1123(98)00043-7.

[20] Dong Z, Rong C. An investigation of alternate behavior of corrosion and fatigue of LY12CZ aluminum alloy. In: Proceedings of the 9th international conference on aluminium alloys. Institute of Materials Engineering Australasia Ltd; 2004, URL http://www.icaa-conference.net/ICAA9/data/papers/GP%2020.pdf.

[21] Nakano Y, Sandor B. Fatigue behavior of copper with intermediate surface layer removal. J Test Eval 1974;2:16–22. http://dx.doi.org/10.1520/JTE10067J.

[22] Zarandi EP, Skallerud BH. Experimental and numerical study of mooring chain residual stresses and implications for fatigue life. Int J Fatigue 2020;135:105530. http://dx.doi.org/10.1016/j.ijfatigue.2020.105530.

[23] Martinez Perez I, Constantinescu A, Bastid P, Zhang Y-H, Venugopal V. Computational fatigue assessment of mooring chains under tension loading. Eng Fail Anal 2019;106:104043. http://dx.doi.org/10.1016/j.engfailanal.2019.06.073.

[24] Faraday M. VI. Experimental researches in electricity. - Seventh series. Philos Trans R Soc 1834;124:77–122. http://dx.doi.org/10.1098/rstl.1834.0008.

[25] Zhang X, Noel N, Ferrari G, Hoogland M. Corrosion behaviour of mooring chain steel in seawater. In: The 67th annual meeting of the international society of electrochemistry. 2016, URL http://resolver.tudelft.nl/uuid:7eb6d065-cb82-4fbd-955c-822821337c21.

[26] Nevshupa R, Martinez I, Ramos S, Arredondo A. The effect of environmental variables on early corrosion of high–strength low–alloy mooring steel immersed in seawater. Mar Struct 2018;60:226–40. http://dx.doi.org/10.1016/j.marstruc.2018.04.003.

[27] Refait P, Grolleau A-M, Jeannin M, François E, Sabot R. Localized corrosion of carbon steel in marine media: Galvanic coupling and heterogeneity of the corrosion product layer. Corros Sci 2016;111:583–95. http://dx.doi.org/10.1016/j.corsci.2016.05.043.

[28] Fredheim S, Reinholdtsen S-A, Håskoll L, Lie HB. Corrosion fatigue testing of used, studless, offshore mooring chain. In: Proceedings of the ASME 2013 32nd international conference on ocean, offshore and arctic engineering. ASME; 2013, OMAE2013-10609.

[29] Gabrielsen Ø, Larsen K, Reinholdtsen S-A. Fatigue testing of used mooring chain. In: Proceedings of the ASME 2017 36th international conference on ocean, offshore and arctic engineering. ASME; 2017, http://dx.doi.org/10.1115/OMAE2017-61382.
[30] Han SM, Benaroya H, Wei T. Dynamics of transversely vibrating beams using four engineering theories. J Sound Vib 1999;225(5):935–88. http://dx.doi.org/10.1006/jsvi.1999.2257.
[31] Pollak RD, Palazotto AN. A comparison of maximum likelihood models for fatigue strength characterization in materials exhibiting a fatigue limit. Probab Eng Mech 2009;24(2):236–41. http://dx.doi.org/10.1016/j.probengmech.2008.06.006.
[32] Recommended practice DNV-RP-C203: Fatigue design of offshore steel structures. Standard, DNV; 2010.
[33] BS 7910:2019, Guide to methods for assessing the acceptability of flaws in metallic structures. Standard, BSI; 2019.
[34] Tada H, Paris PC, Irwin GR. the Stress Analysis of Cracks Handbook. Third Ed.. ASME Press; 2000, http://dx.doi.org/10.1115/1.801535.
[35] Qvale P, Zarandi EP, Ås SK, Skallerud BH. Digital image correlation for continuous mapping of fatigue crack initiation sites on corroded surface from offshore mooring chain. Int J Fatigue 2021;151:106350. http://dx.doi.org/10.1016/j.ijfatigue.2021.106350.
[36] Zarandi EP, Skallerud BH. Cyclic behavior and strain energy-based fatigue damage analysis of mooring chains high strength steel. Mar Struct 2020;70:102703. http://dx.doi.org/10.1016/j.marstruc.2019.102703.